

Nonlinear shear and elongational rheology of model polymer melts by non-equilibrium molecular dynamics

P.J. Daivis^{a,*}, M.L. Matin^a, B.D. Todd^b

^a Department of Applied Physics, RMIT University, GPO Box 2476V, Melbourne, Vic. 3001, Australia

^b Centre for Molecular Simulation, School of Information Technology, Swinburne University of Technology, P.O. Box 218, Hawthorn, Vic. 3122, Australia

Received 23 October 2002; received in revised form 28 November 2002

Abstract

We present the results of non-equilibrium molecular dynamics simulations of planar shear flow and planar elongational flow of melts of model linear chain molecules, in which the number of beads per molecule is varied from $N = 4$ to 50. The shear viscosity η , normal stress coefficients Ψ_1 and Ψ_2 , and the two planar elongational viscosities η_1 and η_2 have been computed as a function of strain rate. The results are analysed using the third order retarded motion expansion (RME). The limiting zero strain rate values of the viscosity ratios agree with their expected values: $\eta_1/\eta = 4$ and $\eta_2/\eta_1 = 0.5$. At low N , values of the coefficient of the lowest order nonlinear term in the RME obtained independently from the shear flow simulations and the elongational flow simulations also agree. However, the consistency check fails for a higher order retarded motion coefficient. This is attributed to insufficient data at low strain rates for the higher values of N . The N -dependence of the viscosities and normal stress coefficients as well as higher order RME constants is studied. We find that the zero strain rate values of the shear viscosity and both elongational viscosities are approximately proportional to N and the limiting values of the first and second normal stress coefficients Ψ_1 and Ψ_2 are approximately proportional to N^3 . The higher order RME constants have exponents nearer to 6.

© 2003 Elsevier Science B.V. All rights reserved.

PACS: 83.10.Mj; 83.50.Ax; 83.50.Jf; 83.60.Rs; 83.80.Sg

Keywords: Elongational flow; Shear flow; Retarded motion expansion; Rouse model; Bead rod model polymer; Non-equilibrium molecular dynamics

1. Introduction

Non-equilibrium molecular dynamics simulation [1,2] is increasingly becoming recognized as a useful tool for investigations of the rheology of model polymer melts and solutions. Examples of

* Corresponding author.

E-mail address: peter.daivis@rmit.edu.au (P.J. Daivis).

investigations of polymer rheology using this technique that have recently been published include a study of the crossover from Rouse to reptation dynamics [3], computation of the viscometric functions of a short-chain polyethylene melt in steady and transient shear [4,5], and an investigation of the stress-optical law for a polymer melt in transient uniaxial elongation [6]. Most previous work has been concerned with planar shear flow (PSF), and when elongational flow has been studied, it has usually only been possible to perform simulations of transient elongation over a restricted timescale.

Recent advances in the development of non-equilibrium molecular dynamics simulation methods for simulating planar elongational flow (PEF) [7–10] have made it possible to simulate planar elongational flow in the steady state by the use of boundary conditions that are periodic in both space and time [11]. This development has opened the way for studies that compare the viscometric functions in steady planar shear flow with those in steady planar elongational flow, to quantitatively assess the performance of various constitutive relations, both from the continuum and molecular point of view.

We have recently compared the results of planar elongational flow and planar shear flow simulations of atomic and low molecular weight molecular fluids [12] and found that the atomic fluid was the only one for which the Reiner–Rivlin equation was able to describe the stress tensor in both planar shear flow and planar elongational flow. With increasing molecular length, the departure from this simple behavior increased. The failure of the Reiner–Rivlin equation to describe steady shear flow of polymeric liquids is usually attributed to its neglect of memory, or equivalently elastic effects, in shear flow [13–15]. The simplest generalization of the Reiner–Rivlin equation that includes both nonlinearity and memory effects is the retarded motion expansion (RME) [15]. We have recently presented a preliminary report on the application of the RME to the analysis of the viscometric functions of a diatomic fluid [16]. In this paper we extend the previous investigation to study longer molecules. Here, the number of sites per molecule, N , is varied from 4 up to 50. We present results for the usual viscometric functions in planar shear flow as well as the two less frequently studied planar elongational viscosities and analyse the results in terms of the RME. We also examine the behavior of the limiting zero shear rate values of these quantities in terms of the Rouse model. A more detailed discussion of conformational, thermodynamic and other results not discussed here is given in the Ph.D. Thesis of Martin [17].

2. Molecular model and simulation technique

2.1. Molecular model

The molecular model that we have used in our simulations is a bead rod model with truncated and shifted Lennard–Jones (LJ) interactions between all beads (sites) except those which are bonded to each other within a molecule. The potential energy function is given by

$$\phi(r_{ij}) = \begin{cases} 4\epsilon \left[\left(\frac{\sigma}{r_{ij}} \right)^{12} - \left(\frac{\sigma}{r_{ij}} \right)^6 \right] - \phi_c, & r_{ij} \leq r_c \\ 0, & r_{ij} > r_c \end{cases} \quad (1)$$

where r_{ij} is the separation of two interaction sites, ϵ the potential well depth and σ is the value of r_{ij} at which the unshifted potential is zero. The shift ϕ_c , which is equal to the value of the unshifted potential at the cutoff $r_{ij} = r_c$, is introduced to eliminate the discontinuity in the potential energy. At distances

greater than the cutoff distance r_c , the potential is zero. For this set of simulations, we have taken the cutoff point for the potential to be the position of the minimum in the LJ potential, $r_c = 2^{1/6}\sigma$. An LJ potential with this truncation point is often known as the WCA potential [18], and it results in purely repulsive interactions. This potential is convenient for computational work because it is short-ranged, and therefore computationally undemanding, but still retains the essential physics, i.e. the repulsive (excluded volume) interaction.

Each molecule consists of N interaction sites of equal mass $m_{i\alpha}$ interacting via the shifted WCA interaction, and joined by rigidly constrained bonds of length $l = \sigma$. The equilibrium equation of state of this model has been studied by Chang and Kim [19]. A similar model that is identical apart from the choice of cutoff distance r_c has been studied by Johnson, Muller and Gubbins [20].

In the remainder of this paper, we express all quantities in terms of site reduced units in which the reduction parameters are the Lennard–Jones interaction parameters ϵ and σ and the mass, $m_{i\alpha}$, of site α on molecule i . In our model, all of the $m_{i\alpha}$ are equal ($m_{i\alpha} = m$). In terms of the corresponding quantities in real units, the reduced temperature T^* is given by $T^* = k_B T / \epsilon$, the density by $\rho^* = \rho \sigma^3 / m$, the pressure by $p^* = p(\sigma^3 / \epsilon)$, the energy by $E^* = E / \epsilon$, and time by $t^* = t / (\sigma(m / \epsilon)^{1/2})$. Reduced strain rates are given by, e.g. $\dot{\gamma}^* = \dot{\gamma} \sigma(m / \epsilon)^{1/2}$. The asterisk denoting reduced quantities will be dropped from here on.

2.2. Equations of motion

In this paper, we study planar shear flow (PSF) and planar elongational flow (PEF). The velocity gradient tensor $\nabla \mathbf{u}$ for each flow is given by

$$\nabla \mathbf{u} = \begin{bmatrix} \dot{\epsilon} & 0 & 0 \\ \dot{\gamma} & -\dot{\epsilon} & 0 \\ 0 & 0 & 0 \end{bmatrix}, \quad (2)$$

where $\dot{\gamma} = 0$ for planar elongational flow and $\dot{\epsilon} = 0$ for planar shear flow.

We use the molecular version of the SLLOD [1] equations of motion given by

$$\dot{\mathbf{r}}_{i\alpha} = \frac{\mathbf{p}_{i\alpha}}{m_{i\alpha}} + \mathbf{r}_i \cdot \nabla \mathbf{u}, \quad (3)$$

$$\dot{\mathbf{p}}_{i\alpha} = \mathbf{F}_{i\alpha}^{\text{LJ}} + \mathbf{F}_{i\alpha}^{\text{C}} - \frac{m_{i\alpha}}{M_i} \mathbf{p}_i \cdot \nabla \mathbf{u} - \zeta^{\text{M}} \frac{m_{i\alpha}}{M_i} \mathbf{p}_i, \quad (4)$$

where $\mathbf{r}_{i\alpha}$ and $\mathbf{p}_{i\alpha}$ represent the position and thermal momentum of site α of molecule i , \mathbf{r}_i represents the position of the centre of mass of molecule i , $m_{i\alpha}$ is the mass of site $i\alpha$, $\mathbf{F}_{i\alpha}^{\text{LJ}}$ represents the sum of all LJ type forces on site α of molecule i and $\mathbf{F}_{i\alpha}^{\text{C}}$ represents the sum of all bond length constraint forces on site α of molecule i . ζ^{M} is the thermostat multiplier, given by

$$\zeta^{\text{M}} = \frac{\sum_{i=1}^{N_m} 1/M_i (\mathbf{F}_i \cdot \mathbf{p}_i - \mathbf{p}_i \cdot \nabla \mathbf{u} \cdot \mathbf{p}_i)}{\sum_{i=1}^{N_m} 1/M_i \mathbf{p}_i^2}, \quad (5)$$

where $\mathbf{p}_i = \sum \mathbf{p}_{i\alpha}$ represents the centre of mass momentum of molecule i , M_i the mass of molecule i and N_m is the number of molecules in the system. This expression for ζ^{M} is derived from Gauss' principle of least constraint, and acts to keep the molecular centre of mass kinetic temperature T^{M} constant, rather

than the atomic or site temperature. Here we define T^M by

$$T^M = \frac{1}{k_B f} \sum_{i=1}^{N_m} \frac{p_i^2}{M_i}, \quad (6)$$

where f represents the number of translational centre of mass degrees of freedom, which depends on the total number of sites and the number of constraints (holonomic and non-holonomic) on the system. This algorithm, including the details of the constraint algorithm, has been discussed previously [21–23].

Note that in the equations of motion, the same strain rate and thermostat terms are applied to all sites on a given molecule. This means that they only affect the centre of mass degrees of freedom and can not interfere with intramolecular (particularly the rotational) degrees of freedom. Alternative forms of the equations of motion can be applied (for example atomic shear with an atomic thermostat), but they can result in a non-zero antisymmetric stress and artificially enhanced orientational ordering. We refer the reader to previous work [24–27] on the subtle but important issues involved in the application of homogeneous thermostats to flowing molecular fluids. The combination of centre of mass molecular shear (or elongation) with a molecular centre of mass thermostat seems to be a simple choice that suffers minimally from the distortions associated with incorrect assumptions about the streaming velocity. Recent work on the development of configurational thermostats [28], which make no assumptions about the streaming velocity, may provide an improvement on the molecular centre of mass thermostat used here. For our current purposes, the molecular centre of mass thermostat will suffice, particularly for strain rates below approximately 1, where all thermostats give identical results.

The SLLOD equations of motion conserve the total peculiar momentum of the system if it has been initialized to zero and the equations of motion are solved exactly. However, we have recently found that when the SLLOD equations of motion are solved numerically for elongational flow, any small error due to unavoidable discretization and finite precision arithmetic errors in the component of the total momentum in the contracting direction can grow exponentially, resulting in catastrophic failure of momentum conservation [10]. This failure in the numerical solution of the equations of motion is easily prevented by initializing the total momentum to zero as usual, and then subtracting any change in the total momentum from the system at each timestep. This very small correction has no effect on the results except to prevent the exponential growth of the numerical error in the momentum. However, it is important to check that the numerical solution of the equations of motion conserves momentum over short times before applying this correction.

Our algorithm for constant (N, V, T^M) simulations of Lennard–Jones chain molecules undergoing shear and elongational flow is based on the Evans, Edberg and Morriss algorithm for shear flow of molecular fluids [21–23], which we have substantially modified by including Kraynik–Reinelt periodic boundary conditions [11] for elongational flow and cell code for efficient neighbour list construction. The details of our implementation of the Kraynik–Reinelt periodic boundary conditions and our cell neighbour list algorithm for planar elongational flow simulations have been published separately [7,8,16].

2.3. Simulation details

Simulations of steady state shear and elongational flow were performed for systems with the simulation parameters summarised in Table 1. Equilibrium configurations of the longer molecules at liquid densities are sometimes difficult to prepare. We found the following method to be very effective. We prepared

Table 1
Simulation parameters

N	N_m	Bond length	LJ cutoff	Time step	T	ρ
4, 10, 20	500	1.0	$2^{1/6}$	0.001	1.00	0.84
50	256	1.0	$2^{1/6}$	0.004	1.00	0.84

a system at low density with the chains initially folded and placed on face centred cubic lattice sites with a randomly chosen initial velocity given to each molecule (equal for all sites) so as to achieve the correct molecular centre of mass kinetic temperature. Then we applied a low strain rate bulk deformation (isotropic compression) to the system using the SLLOD equations of motion for a predetermined time to achieve the desired density. The system was then equilibrated at the required temperature. For shear and elongational flow simulations, block averages of the properties were monitored until the steady state was reached before production runs were commenced. This took from approximately 10 reduced time units for the short-chains at high strain rates to approximately 4000 time units for the long chains at low strain rates. The length of production runs also varied according to chain length and strain rates, the maximum value being approximately 4000 time units for the long chains at low strain rates. The timestep was increased from 0.001 to 0.004 with no noticeable deterioration in the stability of the five-value Gear predictor corrector differential equation solver to obtain better statistical averages for long molecules.

3. Viscometric functions

The pressure tensor in the atomic representation (assuming atomic or interaction site localization of the translational momentum density) was calculated for all fluids from

$$\mathbf{P}^A V = \left\langle \sum_{i=1}^{N_m} \sum_{\alpha=1}^N \frac{\mathbf{p}_{i\alpha} \mathbf{p}_{i\alpha}}{m_{i\alpha}} - \frac{1}{2} \sum_{i=1}^{N_m} \sum_{\alpha=1}^N \sum_{j \neq i}^{N_m} \sum_{\beta=1}^N \mathbf{r}_{i\alpha j\beta} \mathbf{F}_{i\alpha j\beta} - \sum_{i=1}^{N_m} \sum_{\alpha=1}^{N-2} \sum_{\beta=\alpha+2}^N \mathbf{r}_{i\alpha i\beta} \mathbf{F}_{i\alpha i\beta} + \sum_{i=1}^{N_m} \sum_{\alpha=1}^N \mathbf{r}_{i\alpha} \mathbf{F}_{i\alpha}^C \right\rangle, \quad (7)$$

where $\mathbf{F}_{i\alpha j\beta}$ represents the LJ force on site α of molecule i due to site β of molecule j , and $\mathbf{F}_{i\alpha}^C$ represents the total bond constraint force on site α of molecule i . $\mathbf{r}_{i\alpha j\beta} = \mathbf{r}_{j\beta} - \mathbf{r}_{i\alpha}$ is the minimum image separation of site α of molecule i from site β of molecule j . The second and third terms represent the intermolecular and intramolecular contributions to the pressure tensor, respectively. The angular brackets denote an average over the non-equilibrium steady state.

The pressure tensor in the molecular representation was calculated using the expression

$$\mathbf{P}^M V = \left\langle \sum_{i=1}^{N_m} \frac{\mathbf{p}_i \mathbf{p}_i}{M_i} - \frac{1}{2} \sum_{i=1}^{N_m} \sum_{\alpha=1}^N \sum_{j \neq i}^{N_m} \sum_{\beta=1}^N \mathbf{r}_{ij} \mathbf{F}_{i\alpha j\beta}^{\text{inter}} \right\rangle, \quad (8)$$

where, as before, \mathbf{p}_i represents the total peculiar momentum of molecule i , as defined by the equations of motion, and $\mathbf{F}_{i\alpha j\beta}^{\text{inter}}$ represents the intermolecular force on site $i\alpha$ due to site $j\beta$. $\mathbf{r}_{ij} = \mathbf{r}_j - \mathbf{r}_i$ is the

minimum image separation of the centre of mass of molecule i from the centre of mass of molecule j . Care must be taken in the evaluation of this expression in cases where it is possible for sites on two different periodic images of the same molecule to interact. In such cases, the correct value of $\mathbf{r}_{ij} = \mathbf{r}_j - \mathbf{r}_i$ corresponding to the particular images of molecules i and j in $\mathbf{F}_{i\alpha j\beta}^{\text{inter}}$ must be used in the computation of \mathbf{P}^M . This is particularly important in simulations of planar elongational flow for long molecules, because the minimum distance between different periodic images of the same molecule is smaller in elongation than in shear.

This definition of the molecular pressure tensor assumes that the molecular peculiar momenta are correctly defined by Eq. (3). If all forces are central forces, the instantaneous atomic pressure tensor is symmetric, but the instantaneous molecular pressure tensor is not [22]. However the average of the molecular pressure tensor should be symmetric and equal to the atomic pressure tensor in a steady state, provided that no external torques act on the molecules. (This condition is not satisfied by atomic thermostats [24,25].) The pressure p represents the isotropic part of the pressure tensor, given by $p = 1/3\text{Tr}(\mathbf{P})$. It is now well established that both the pressure and the internal energy are observed to vary strongly with strain rate in NEMD simulations. This occurs because the strain rates that are easily studied by NEMD are of order 1 in reduced units, which corresponds to approximately 10^{12} s^{-1} in real units for liquid Argon. At these extremely high strain rates, the radial distribution function becomes strongly distorted, affecting the potential energy and both the diagonal and off-diagonal elements of the pressure tensor and leading to non-Newtonian behavior. On the other hand, the physical mechanism for the experimentally observed nonlinear behavior of polymeric fluids is expected to be mainly entropic, being associated with molecular alignment and conformational changes. We expect a small or negligible change in the pressure and potential energy of a polymeric fluid at experimentally accessible strain rates. In addition, rheology experiments are normally performed with the substance under investigation having one surface in equilibrium with the atmosphere. To more closely approximate real experimental conditions, we have therefore also performed some simulations keeping the zz element of the pressure tensor constant as the strain rate is increased. Under these conditions, we observe shear dilatancy—a decrease in the density of the fluid with increasing strain rate. It has previously been shown that constant pressure simulations produce results more similar to experimental results than constant volume simulations [29]. Note however, that in the results reported here, the density—not the pressure, is kept constant as the chain length is increased at zero strain rate.

For our shear flow geometry, defined by Eq. (2) with $\dot{\epsilon} = 0$, the generalized non-Newtonian shear viscosity of a fluid subject to planar shear flow is defined as

$$\eta = -\frac{P_{xy} + P_{yx}}{2\dot{\gamma}}. \quad (9)$$

This equation applies when either the atomic or molecular pressure tensors are used.

Fig. 1 shows the strain rate dependence of the shear viscosity for different chain lengths. We observe a Newtonian region followed by a region of shear thinning that extends over one decade of strain rate in the case of the four site molecules, increasing to three decades of shear thinning behavior in the case of the 50-site molecules. As expected, the critical strain rate for the onset of shear thinning decreases with increasing N . We also observe the onset of shear thickening at higher strain rates (only reached for the 4- and 10-site molecules) when the simulations are performed at constant volume, but not when they are performed at constant P_{zz} . This shear thickening behavior under constant volume conditions is not always observed, due to the subtle but important differences in the thermostating techniques used in different

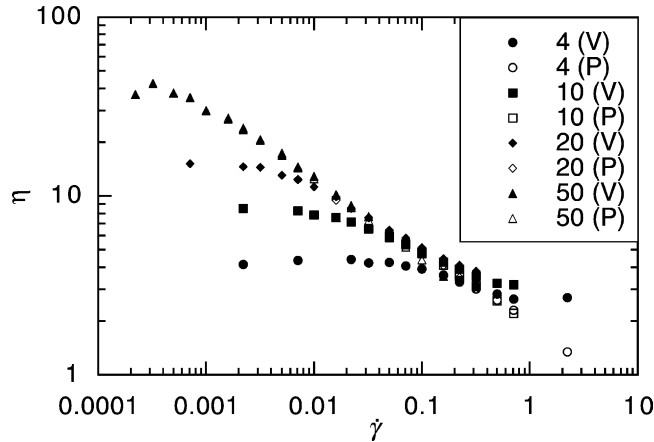


Fig. 1. Strain rate dependence of the shear viscosity for different chain lengths. Results obtained at constant volume are represented by filled symbols and results obtained at constant P_{zz} are represented by open symbols. Error bars are approximately the same size as the symbols and have been omitted for clarity.

NEMD studies mentioned earlier. At the high strain rates at which shear thickening is observed in our constant volume simulations, the details of the thermostatting method become important. It is usually observed that shear thickening is absent in constant volume simulations that employ atomic thermostats [26], due to the enhanced orientational ordering and reduced molecular rotation associated with the atomic thermostatting method.

The two normal stress coefficients defined as

$$\Psi_1 = \frac{P_{yy} - P_{xx}}{\dot{\gamma}^2} \quad (10)$$

and

$$\Psi_2 = \frac{P_{zz} - P_{yy}}{\dot{\gamma}^2} \quad (11)$$

are shown in Fig. 2 and 3. Both of these quantities exhibit strain rate dependence in qualitative agreement with experimental data on polymer melts. In particular, Ψ_2 is negative and the zero shear rate limit of the ratio of the normal stresses Ψ_2/Ψ_1 varies from approximately 0.4 at $N = 2$ down to 0.1–0.2 at $N = 50$. These values are consistent with results of other simulation studies [4,30] and the long chain values are consistent with typical experimental values for polymer melts [15]. The differences between constant pressure and constant volume results are clearly less significant for the normal stress coefficients than for the shear viscosity.

The results of the simulations in which P_{zz} was kept constant as the strain rate was increased suggest that the shear viscosity and the two normal stress coefficients follow power laws at high shear rates. The results of linear fits to log–log plots of the highest strain rate data for each value of N are given in Table 2. The values of the exponents are within the range of experimental values for polymer melts and concentrated solutions [15]. It is also interesting to note that these values are similar to those obtained in previous computer simulation studies (for example [4,30]). This occurs despite two major differences between our simulation methodology and that employed in the other studies. The first difference is our

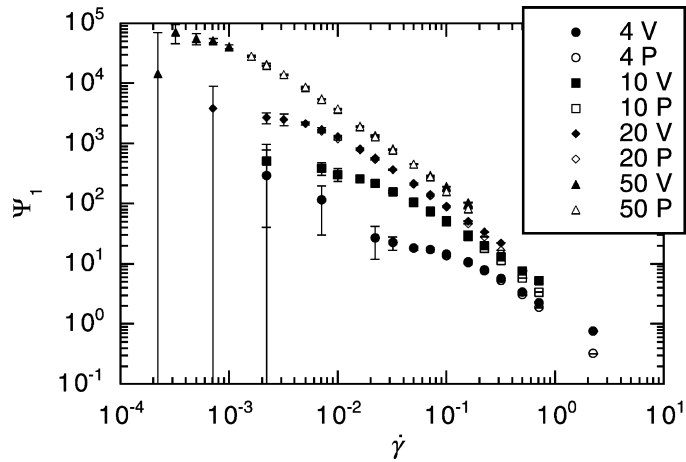


Fig. 2. Strain rate dependence of the first normal stress coefficient in steady shear flow for different chain lengths. Results obtained at constant volume are represented by filled symbols and results obtained at constant P_{zz} are represented by open symbols.

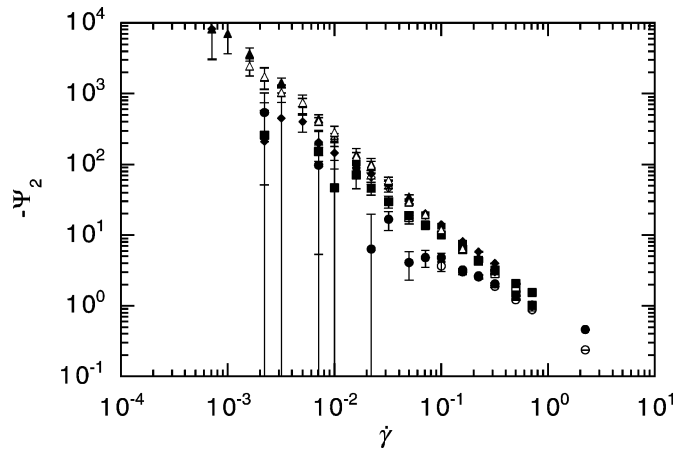


Fig. 3. Strain rate dependence of minus the second normal stress coefficient in steady shear flow for different chain lengths. Symbols have the same meaning as previously. The two lowest shear rate values of Ψ_2 for the $N = 50$ chains were negative and had very large uncertainties so they have been omitted.

Table 2

Results of fits of the form $\eta = k_1 \dot{\gamma}^{n_1}$, $\Psi_1 = k_2 \dot{\gamma}^{n_2}$ and $-\Psi_2 = k_3 \dot{\gamma}^{n_3}$ to constant pressure shear viscosities, first normal stress coefficients and second normal stress coefficients in the power law region

N	k_1	n_1	k_2	n_2	k_3	n_3
4	1.95	-0.45	1.08	-1.51	0.58	-1.10
10	1.91	-0.43	2.14	-1.42	0.68	-1.21
20	1.86	-0.42	3.78	-1.34	0.72	-1.24
50	1.58	-0.45	7.46	-1.35	0.51	-1.36

use of a molecular thermostat and the second is that we have allowed for shear dilatancy by performing simulations at constant pressure. Both of these differences become significant at high shear rates, but their effects on the viscometric functions appear to approximately cancel, so that our results for constant pressure simulations with a molecular thermostat are qualitatively similar to the results of other studies that used an atomic thermostat and constant volume. These methodological differences become irrelevant at the strain rates at which the constant volume and constant pressure results shown in Figs. 1 and 6 agree.

For planar elongational flow, defined by Eq. (2) with $\dot{\gamma} = 0$, the two elongational viscosities may be defined as

$$\eta_1 = \frac{P_{yy} - P_{xx}}{\dot{\epsilon}} \quad (12)$$

and

$$\eta_2 = \frac{P_{yy} - P_{zz}}{\dot{\epsilon}}. \quad (13)$$

The two elongational viscosities are shown in Figs. 4 and 5. The constant pressure curves for η_1 at $N > 10$ display all of the qualitative features exhibited by experimental data for the elongational viscosity of polymeric liquids—a Newtonian region, followed by a strongly increasing viscosity at low values of the strain rate, peaking at a value that increases with increasing N , and then a region of “elongation thinning” [31]. The second planar elongational viscosity is very rarely measured, and then only transient measurements are available, e.g. [32]), so we have no reliable experimental data with which to compare our steady elongation results.

To a first approximation, it might be expected that in steady planar elongational flow, the magnitude of the decrease in P_{xx} should equal the magnitude of the increase in P_{yy} , while P_{zz} remains approximately constant. This would imply that $\eta_2/\eta_1 = 0.5$. To test the range over which this approximation is satisfied, we have plotted the ratio of the two planar elongational viscosities as a function of strain rate in Fig. 6, which shows that the range over which the limiting behavior is observed decreases with increasing N . It also reveals that the ratio of the two viscosities has a broad minimum for $N = 4$ which becomes an

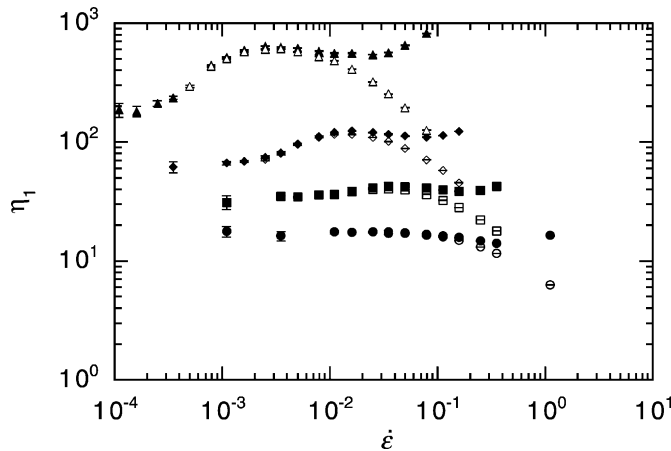


Fig. 4. Strain rate dependence of the first planar elongational viscosity in steady planar elongational flow for different chain lengths. Symbols have the same meaning as defined in Figs. 1 and 2. As before, the filled symbols represent the results of constant volume simulations and the open symbols represent the results of simulations with constant P_{zz} .

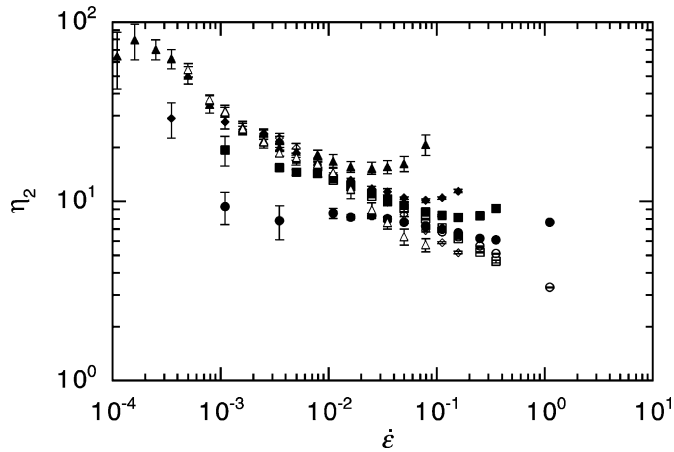


Fig. 5. Strain rate dependence of the second planar elongational viscosity in steady planar elongational flow for different chain lengths. Symbols have the same meaning as defined in Figs. 1 and 2. As before, the filled symbols represent the results of constant volume simulations and the open symbols represent the results of simulations with constant P_{zz} .

extended region of constant η_2/η_1 as N is increased. Further analysis of the $N = 10, 20, 50$ data was performed by approximating the high $\dot{\epsilon}$ curve in Fig. 6 by two straight lines, one of them with zero gradient representing an asymptotic high strain rate value $(\eta_2/\eta_1)_\infty$ and the other representing the approximately linear behavior of the ratio at intermediate $\dot{\epsilon}$ values. The intersection of these two lines provides us with an estimate of the critical value $\dot{\epsilon}_c$ of $\dot{\epsilon}$ at which the crossover to strain rate independence occurs. Both of these quantities obey power laws in N given by

$$\left(\frac{\eta_2}{\eta_1}\right)_\infty = 3.95N^{-1.26} \tag{14}$$

$$\dot{\epsilon}_c = 7.94N^{-2.30}. \tag{15}$$

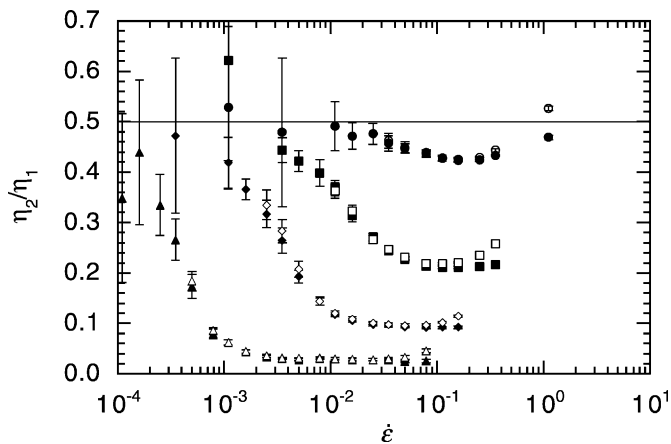


Fig. 6. Strain rate dependence of the ratio of the two elongational viscosities in steady planar elongational flow for different chain lengths. Symbols have the same meaning as defined in Figs. 1 and 2. The expected limiting value at zero strain rate is 0.5.

4. Reiner–Rivlin equation

The Reiner–Rivlin equation [13–15] expresses the pressure tensor in terms of the symmetric strain rate tensor \mathbf{D}

$$\mathbf{P} = p\mathbf{1} - \phi_1(\text{II}, \text{III})\mathbf{D} - \phi_2(\text{II}, \text{III})\mathbf{D}^2, \quad (16)$$

where the symmetric strain rate tensor is defined as

$$\mathbf{D} = \nabla\mathbf{u} + (\nabla\mathbf{u})^T, \quad (17)$$

and the scalar invariants of the strain rate tensor are defined by

$$\text{I} = \text{Tr}(\mathbf{D}), \text{II} = \text{Tr}(\mathbf{D} \cdot \mathbf{D}), \text{III} = \text{Tr}(\mathbf{D} \cdot \mathbf{D} \cdot \mathbf{D}). \quad (18)$$

The first and third scalar invariants are zero for both planar shear flow and planar elongational flow. The second scalar invariant, which is proportional to the rate of heat dissipation in the steady state in both planar shear flow and planar elongational flow, takes the values $\text{II} = 2\dot{\gamma}^2$ for planar shear flow and $\text{II} = 8\dot{\epsilon}^2$ for planar elongational flow.

In previous work [12], we discussed the results of simulations of molecular fluids with N equal to 1, 2 and 4 in planar shear flow and planar elongational flow and we found that for $N = 1$, η and $\eta_1/4$ fell on a universal curve when they were plotted as a function of the second scalar invariant II , in agreement with the Reiner–Rivlin equation. When N was increased, the agreement between the two viscosities became poorer. As we have seen above, the behavior of the two viscosities becomes totally different when N is increased still further. These results confirm the well-known fact that the Reiner–Rivlin equation fails to give an adequate description of elastic fluids in shear flow. Therefore we restrict our application of the Reiner–Rivlin equation to the planar elongational flow results.

The results that we have obtained for the steady planar elongational flow elongational viscosities provide us with an opportunity to evaluate the material functions $\phi_1(\text{II}, \text{III} = 0)$ and $\phi_2(\text{II}, \text{III} = 0)$ in the Reiner–Rivlin equation. Substituting the strain rate tensor for planar elongational flow into Eq. (16) and solving for $\phi_1(\text{II})$ and $\phi_2(\text{II})$, we find

$$\phi_1 = \frac{\eta_1}{2} \quad (19)$$

and

$$\phi_2 = \frac{\eta_1 - 2\eta_2}{8\dot{\epsilon}}. \quad (20)$$

The first of these functions is trivially related to the first elongational viscosity, which is plotted in Fig. 4. The second function, ϕ_2 , is plotted in Fig. 7. This function displays strong elongation thinning, like ϕ_1 , at high strain rates but for $N < 50$ it is approximately constant at low strain rates, which may be a useful property for the description of the elongational rheology of short-chain molecules. For $N = 50$, ϕ_2 has a maximum which could be expected to grow with increasing N . There do not appear to be any reliable experimental data with which we can compare our results for ϕ_2 .

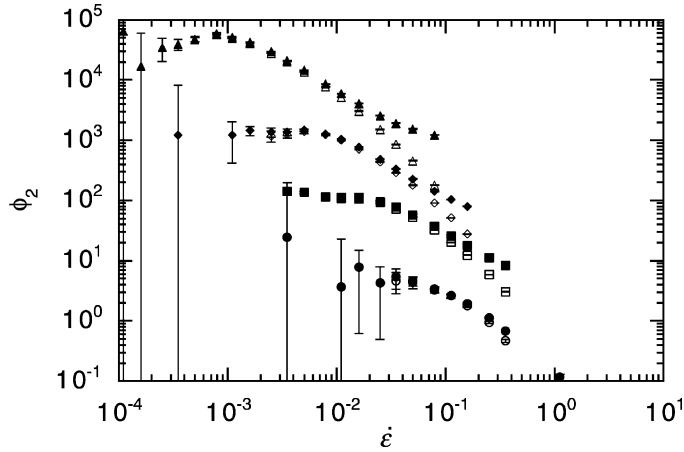


Fig. 7. The Reiner–Rivlin function ϕ_2 , defined by Eq. (20). Symbols have the same meaning as defined in Figs. 1 and 2. Recall that $\Pi = 8\dot{\epsilon}^2$ for planar elongational flow.

5. Retarded motion expansion

The retarded motion expansion (RME) offers a systematic, model-independent description of the low Deborah number behavior of an arbitrary viscoelastic fluid. The details of the retarded motion expansion are given in standard textbooks [15]. The third order retarded motion expansion gives the following expressions for the viscometric functions in planar shear flow

$$\eta = b_1 - 2(b_{12} - b_{1:11})\dot{\gamma}^2 \quad (21)$$

$$\Psi_1 = -2b_2 \quad (22)$$

$$\Psi_2 = b_{11} \quad (23)$$

and the following expressions for the viscometric functions in planar elongational flow

$$\eta_1 = 4b_1 + 16(b_3 - 2b_{12} + 2b_{1:11})\dot{\epsilon}^2 \quad (24)$$

$$\eta_2 = 2b_1 - 4(b_{11} - b_2)\dot{\epsilon} + 8(b_3 - 2b_{12} + 2b_{1:11})\dot{\epsilon}^2 \quad (25)$$

where the b_{ij} coefficients are constants in the RME. These equations show that the initial strain rate dependence of the shear viscosity is expected to be quadratic and the first and second normal stress coefficients should be constant at this level of approximation. Likewise, the two elongational viscosities are expected to be quadratic functions of the strain rate in the third order fluid approximation.

We have evaluated the coefficients in these equations by fitting the low strain rate data with the appropriate polynomial functions using a weighted linear least squares fitting program. The fits were performed several times for each data set, progressively restricting the data to lower maximum strain rates until the systematic deviations from the assumed functional form were minimised and the quality of the fit (as judged by the correlation coefficient) was maximised. Deviations from linearity are far easier to discern than deviations from any other functional form, so wherever it was possible, the data were reworked so that the assumed functional form was linear. For example the first normal stress coefficients were plotted

Table 3
Results of analysis of planar shear flow data using the third order fluid model

N	$b_1 = \eta_0$	$2(b_{12} - b_{1:11})$	$-2b_2 = \Psi_{1,0}$	$-b_{11} = -\Psi_{2,0}$	$b_{11} - b_2$
2	2.957 (2)	5.0 (1)	3.5 (1)	1.49 (8)	0.21 (7)
4	4.26 (3)	37 (4)	19 (3)	4 (2)	6 (3)
10	7.91 (7)	1400 (100)	290 (40)	100 (50)	60 (10)
20	14.6 (2)	50000 (7000)	2800 (400)	400 (100)	700 (100)
50	40.9 (9)	$1.1 (1) \times 10^7$	56000 (8000)	7000 (5000)	18000 (6000)

Data for $N = 2$ are recalculated from our previously published work [16]. The numbers in brackets are uncertainties.

as a function of $\dot{\gamma}^2$ and the limiting zero shear rate value was estimated from the intercept. The results of the data analysis using the third order fluid model are given in Tables 3 and 4.

Several consistency checks on the RME can be made using the planar shear flow and planar elongational flow data in Tables 3 and 4. The values of $b_1 = \eta_0$, the zero strain rate viscosity will be examined first. The limiting values of this quantity calculated from the shear viscosity and the second planar elongational viscosity are in excellent agreement. The agreement between these two values and the one calculated from the first planar elongational viscosity is also good, but at larger chain lengths, the value of b_1 obtained from η_1 is systematically slightly higher than the other two. This may be due to the extremely rapid variation of η_1 with strain rate for large N . Attempts were made to account for the rapid variation in η_1 with strain rate by fitting the data with a quadratic function in $\dot{\epsilon}^2$, however this resulted in no significant improvement in the results. An additional check on the accuracy of our value for η_0 was made by computing the viscosity from the Green–Kubo relation, which gives the viscosity in terms of the integral of the equilibrium stress autocorrelation function [1,29]. The stress autocorrelation function was averaged over 10,000 reduced time units and integrated from zero to 60 reduced time units. We obtained a value of 8.6 ± 0.7 for the 10-site molecules, which agrees with the values given above after taking uncertainties into account.

The values of $(b_{11} - b_2)$ given in Table 3 were calculated directly from the intercepts of linear fits to $(\Psi_1/2 + \Psi_2)$ as a function of $\dot{\gamma}^2$. These values compare well with the values calculated from the values of $-2b_2 = \Psi_{1,0}$ and $-b_{11} = -\Psi_{2,0}$ given in the previous columns, but they have smaller uncertainties and are less affected by rounding and the propagation of errors through intermediate results. These can be compared with the values given in Table 4 from the strain rate dependence of the second planar

Table 4
Results of analysis of planar elongational flow data using the third order fluid model

N	From η_1		From η_2		
	$b_1 = \eta_0$	$b_3 - 2b_{12} + 2b_{1:11}$	$b_1 = \eta_0$	$b_{11} - b_2$	$b_3 - 2b_{12} + 2b_{1:11}$
2	2.965 (5)	-3.2 (3)	2.99 (2)	0.8 (2)	0.2 (8)
4	4.3 (1)	40 (60)	4.20 (5)	4.0 (5)	3.6 (6)
10	8.6 (1)	1000 (100)	7.9 (2)	62 (7)	300 (60)
20	16.5 (3)	77000 (4000)	14.5 (5)	600 (100)	13000 (4000)
50	46 (2)	$26 (1) \times 10^6$	42 (4)	19000 (4000)	$3 (1) \times 10^6$

Data for $N = 2$ are recalculated from our previously published work [16]. The numbers in brackets are uncertainties.

Table 5

Relaxation times and values of the shear rate and elongation rate at which $De = 1$ for different chain lengths

N	$\lambda = -b_2/b_1$	$\dot{\gamma}^*$	$\dot{\epsilon}^*$
2	0.59	0.84	0.42
4	2.2	0.22	0.11
10	18	0.027	0.014
20	96	0.0052	0.0026
50	680	0.00073	0.00037

elongational viscosity. The values of $(b_{11} - b_2)$ obtained from the planar shear flow and planar elongational flow viscometric functions are generally in good agreement, considering the rather large uncertainties.

Another combination of the RME coefficients that can be obtained by two independent methods from our data set is the quantity $(b_3 - 2b_{12} + 2b_{1:11})$, which can be calculated from both the first and second planar elongational viscosities. The two sets of values, shown in Table 3, do not agree for N greater than 4. This is consistent with our previous observation that the poorest estimate of $b_1 = \eta_0$ is the one calculated from η_1 , whereas the estimates of both b_1 and $b_{11} - b_2$ obtained from η_2 agree reasonably well with the planar shear flow data. The most likely reason for this discrepancy is that the planar elongational flow data at low strain rates are still not precise enough and lower strain rates need to be studied. These would be extremely demanding computations. The poor agreement between our two values for $(b_3 - 2b_{12} + 2b_{1:11})$ prevents us from accurately evaluating b_3 , which would be an extremely interesting quantity, because it is the only coefficient in the third order RME expansion that cannot be evaluated from shear flow alone.

The validity of the RME is restricted to values of the Deborah number De significantly less than unity. (Note that we follow Bird et al. [15] in using De as the dimensionless number to describe steady flow, where only one characteristic time can be identified.) A reasonable estimate of De that is valid for both planar shear flow and planar elongational flow is provided by the expression

$$De = \frac{\Psi_{1,0}}{2\eta_0} \sqrt{2\Pi}, \quad (26)$$

where Π is defined by Eq. (18). Relaxation times and values of the shear rate and elongation rate at which $De = 1$ are given in Table 5. In all cases except for $N = 50$, the condition $De \lesssim 1$ was satisfied for the range of the data used to fit the RME expressions. This confirms that lower strain rates need to be studied for the largest chain lengths discussed here in order to better satisfy the requirement that the Deborah number should be small.

6. N -dependence of the RME constants

Kröger et al. [30] have studied the viscometric functions in planar shear flow over a wide range of chain lengths for a similar model to ours at the same temperature and density. The only chain length for which results are available from both studies is $N = 10$. Direct comparison of the two sets of results shows that our zero shear rate viscosity (7.91 ± 0.07) is higher than theirs (7.09 ± 0.09) and that our first normal stress coefficient (290 ± 40) is lower than theirs (425 ± 50). These differences reflect the slight differences between the freely jointed Lennard–Jones chain and the FENE chain models.

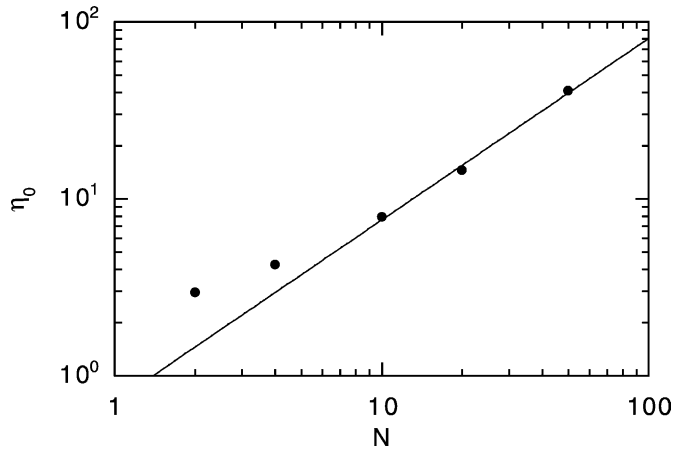


Fig. 8. Chain length dependence of the zero-shear rate viscosity. A power law fit for $N = 10, 20, 50$ gives a slope of 1.03 ± 0.07 , which agrees with the Rouse value of 1 within uncertainties.

More recently, Kröger and Hess [3] found that the crossover from Rouse to reptation dynamics in the viscometric functions occurred at approximately $N_c = 100$, indicating that our results, obtained for a slightly less flexible model chain, are expected to be well below the crossover. For molecules satisfying the condition $N < N_c$ the Rouse model provides us with theoretical predictions for the chain-length dependence of the zero strain rate shear viscosity and the longest intramolecular relaxation time. The shear viscosity is predicted to vary as $\eta \propto N$ and the relaxation time is predicted to vary as $\lambda = \psi_{1,0}/2\eta_0 \propto N^2$, giving $\psi_{1,0} \propto N^3$. These relationships are tested in Figs. 8 and 9. Fig. 8 shows that the Rouse prediction is verified for the three highest chain lengths, but more data for larger N are obviously needed. Fig. 9 shows

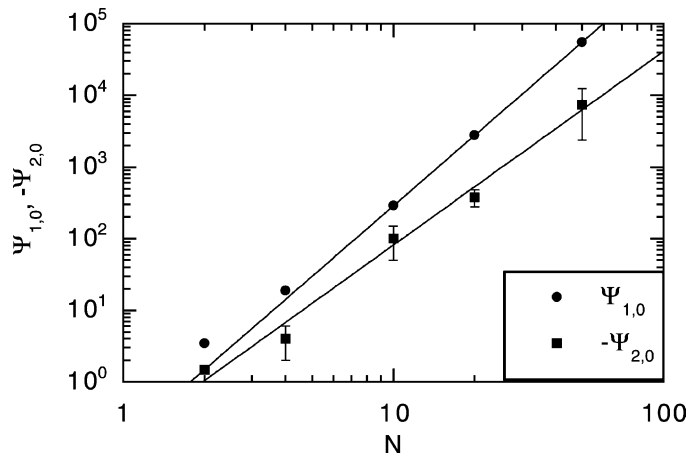


Fig. 9. Chain length dependence of the zero-shear rate limiting values of the first normal stress coefficients $\Psi_{1,0}$ (shown by circles) and the negative of the second normal stress coefficients $-\Psi_{2,0}$ (shown by squares). Power law fits to the data for $N = 10, 20, 50$ give exponents of 3.27 ± 0.01 and 2.7 ± 0.4 , respectively. Error bars for $\Psi_{1,0}$ are the same size as the symbols and have been omitted for clarity.

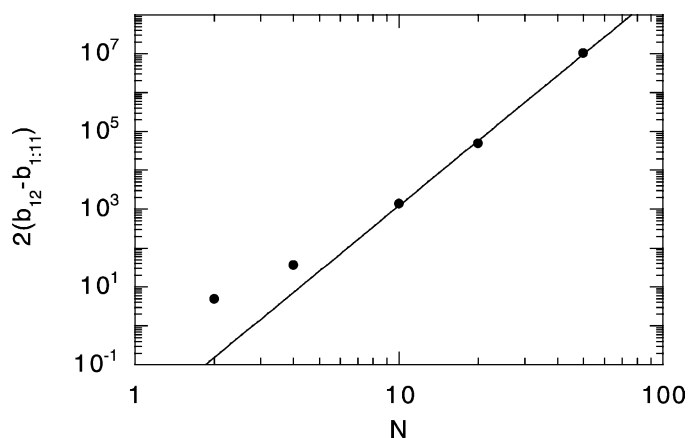


Fig. 10. Chain length dependence of the coefficient on the quadratic term in the third-order fluid expression for the nonlinear shear viscosity. A power law fit to the data for $N = 10, 20, 50$ gives an exponent of 5.6 ± 0.2 .

that the first normal stress coefficient, $\Psi_{1,0}$ varies as $N^{3.27 \pm 0.01}$ and the negative of the second normal stress coefficient, $-\Psi_{2,0}$, varies as $N^{2.7 \pm 0.4}$. The first value is slightly larger than the value of 3.0 predicted by the Rouse model, but the second, for which there is no Rouse model prediction, is within errors of 3.0.

We also have an opportunity to determine the N -dependence of the other RME constants. Fig. 10 shows the N -dependence of the coefficient of the nonlinear term in the third order fluid expression for the shear viscosity given by Eq. (21). A power law fit to the data for $N = 10, 20, 50$ gives an exponent of 5.6 ± 0.2 . The Rouse model does not provide a prediction for the N -dependence of this coefficient. A similar analysis of the RME constant $(b_3 - 2b_{12} + 2b_{1;11})$ can be performed. Despite that fact that the two determinations of this quantity shown in Table 4 do not agree, their N -dependence exponents are quite similar, having values that fall in the region of 6.0 ± 0.3 .

The preceding analysis in terms of the Rouse model presumes that the monomeric friction coefficient is independent of N over the range of the power law fits (i.e. $N = 10, 20, 50$). It is well-known that this quantity varies with N at low values of N and tends toward a constant value at high N and that this should be accounted for in the analysis of viscosity data [33]. It is yet to be determined whether the monomeric friction coefficient has reached its limiting value within the range of N investigated here, but the power laws that we observe for $N > 4$ imply that it has. The glass transition temperature is also unknown for both the freely jointed LJ chain model and the FENE chain model. We note that in recent molecular dynamics studies of the FENE chain model, the value of N_c at which the crossover from Rouse to reptation dynamics occurred for the self diffusion coefficient [34] was found to be far lower (at around 35) than for the zero shear viscosity [3] (around 100). This points to an inconsistency in the interpretation based on the Rouse model. Our results confirm that N_c , as measured by the zero shear rate viscosity (shown in Fig. 8), is greater than 50.

7. Conclusion

The viscometric functions have been determined in steady planar shear flow and planar elongational flow for model Lennard–Jones chains below the entanglement chain length by non-equilibrium molecular

dynamics simulations. The high precision of our results has allowed us to determine the coefficients of the retarded motion expansion coefficients for the third order fluid model. The limiting zero strain rate values of the shear viscosity and the first and second elongational viscosities obey the expected relationships, and the leading order nonlinear terms in the retarded motion expansion satisfy a consistency check between the values obtained for the two different flows. The chain length dependence of the retarded motion coefficients has also been determined. The chain length dependence of the zero shear rate viscosity is consistent with the prediction of the Rouse model, $\eta \propto N^1$ and the chain length dependence of the first normal stress coefficient is also close to the Rouse model prediction. The chain length dependence of the higher order coefficients in the third order retarded motion expansion, for which there are no theoretical predictions, has also been determined, giving exponents nearer to 6.

The results that we have obtained confirm the internal consistency of the third order fluid model in its description of steady shear and elongational flows—something that is very difficult to achieve experimentally due to the transient nature of most elongational flow experiments.

In future work, we intend to compare our results with molecular theories and extend our investigations to smaller strain rates and larger chain lengths.

Acknowledgements

This work was supported by the Cooperative Research Centre for Polymers. We would like to thank the CSIRO/Bureau of Meteorology High Performance Computing and Communications Centre and the Australian and Victorian Partnerships for Advanced Computing for generous allocations of computer time. We also thank Prof. G. McKinley and Prof. R. Tanner for helpful suggestions.

References

- [1] D.J. Evans, G.P. Morriss, *Statistical Mechanics of Nonequilibrium Liquids*, Academic Press, New York, 1990.
- [2] M.P. Allen, D.J. Tildesley, *Computer Simulation of Liquids*, Clarendon Press, Oxford, 1987.
- [3] M. Kröger, S. Hess, Rheological evidence for a dynamical crossover in polymer melts via nonequilibrium molecular dynamics, *Phys. Rev. Lett.* 85 (2000) 1128.
- [4] J.D. Moore, S.T. Cui, H.D. Cochran, P.T. Cummings, A molecular dynamics study of a short-chain polyethylene melt. I. Steady-state shear, *J. Non-Newtonian Fluid Mech.* 93 (2000) 83.
- [5] J.D. Moore, S.T. Cui, H.D. Cochran, P.T. Cummings, A molecular dynamics study of a short-chain polyethylene melt. II. Transient response upon onset of shear, *J. Non-Newtonian Fluid Mech.* 93 (2000) 101.
- [6] M. Kröger, C. Luap, R. Muller, Polymer melts under uniaxial elongational flow: stress-optical behavior from experiments and non-equilibrium molecular dynamics computer simulations, *Macromolecules* 30 (1997) 526.
- [7] B.D. Todd, P.J. Davis, Nonequilibrium molecular dynamics simulations of planar elongational flow with spatially and temporally periodic boundary conditions, *Phys. Rev. Lett.* 81 (1998) 1118.
- [8] B.D. Todd, P.J. Davis, A new algorithm for unrestricted duration nonequilibrium molecular dynamics simulations of planar elongational flow, *Comput. Phys. Commun.* 117 (1999) 191.
- [9] A. Baranyai, P.T. Cummings, Steady state simulation of planar elongational flow by nonequilibrium molecular dynamics, *J. Chem. Phys.* 110 (1999) 42.
- [10] B.D. Todd, P.J. Davis, The stability of nonequilibrium molecular dynamics simulations of elongational flows, *J. Chem. Phys.* 112 (2000) 40.
- [11] A.M. Kraynik, D.A. Reinelt, Extensional motions of spatially periodic lattices, *Int. J. Multiphase Flow* 18 (1992) 1045.
- [12] M.L. Matin, P.J. Davis, B.D. Todd, Comparison of planar shear flow and planar elongational flow for systems of small molecules, *J. Chem. Phys.* 113 (2000) 9122 [Erratum: M. L. Matin, P. J. Davis, B. D. Todd, *J. Chem. Phys.* 115 (2001) 5338].

- [13] A.S. Lodge, *Body Tensor Fields in Continuum Mechanics*, Academic Press, New York, 1974.
- [14] W.R. Schowalter, *Mechanics of Non-Newtonian Fluids*, Pergamon Press, Oxford, 1978.
- [15] R.B. Bird, R.C. Armstrong, O. Hassager, *Dynamics of Polymeric Liquids*, vol. 1, Wiley, New York, 1987.
- [16] M.L. Matin, P.J. Daivis, B.D. Todd, Cell neighbour list method for planar elongational flow: rheology of a diatomic fluid, *Comput. Phys. Commun.*, 2002, submitted for publication.
- [17] M.L. Matin, *Molecular simulation of polymer rheology*, Ph.D. Thesis, RMIT University, 2001.
- [18] J.D. Weeks, D. Chandler, H.C. Andersen, Role of repulsive forces in determining the equilibrium structure of simple liquids, *J. Chem. Phys.* 54 (1971) 5237.
- [19] J. Chang, Molecular dynamic simulation and equation of state of Lennard–Jones chain fluids, *Korean J. Chem. Eng.* 15 (1998) 544.
- [20] J.K. Johnson, E.A. Muller, K.E. Gubbins, Equation of state for Lennard–Jones chains, *J. Phys. Chem.* 98 (1994) 6413.
- [21] R. Edberg, D.J. Evans, G.P. Morriss, Constrained molecular dynamics: simulations of liquid alkanes with a new algorithm, *J. Chem. Phys.* 84 (1986) 6933.
- [22] R. Edberg, G.P. Morriss, D.J. Evans, Rheology of *n*-alkanes by nonequilibrium molecular dynamics, *J. Chem. Phys.* 86 (1987) 4555.
- [23] G.P. Morriss, D.J. Evans, A constraint algorithm for the computer simulation of complex molecular liquids, *Comput. Phys. Commun.* 62 (1991) 267.
- [24] K.P. Travis, P.J. Daivis, D.J. Evans, Computer simulation algorithms for molecules undergoing planar Couette flow: a nonequilibrium molecular dynamics study, *J. Chem. Phys.* 103 (1995) 1109.
- [25] K.P. Travis, P.J. Daivis, D.J. Evans, Thermostats for molecular fluids undergoing shear flow: application to liquid chlorine, *J. Chem. Phys.* 103 (1995) 10638 [Erratum: *J. Chem. Phys.* 105 (1996) 3893].
- [26] K.P. Travis, D.J. Evans, On the rheology of *n*-eicosane, *Mol. Sim.* 17 (1996) 157.
- [27] P. Padilla, S. Toxvaerd, Simulating shear flow, *J. Chem. Phys.* 104 (1996) 5956.
- [28] J. Delhommelle, D.J. Evans, Comparison of thermostatting mechanisms in NVT and NPT simulations of decane under shear, *J. Chem. Phys.* 115 (2001) 43.
- [29] P.J. Daivis, D.J. Evans, Comparison of constant pressure and constant volume non-equilibrium simulations of sheared model decane, *J. Chem. Phys.* 100 (1994) 541.
- [30] M. Kröger, W. Loose, S. Hess, Rheology and structural changes of polymer melts vis nonequilibrium molecular dynamics, *J. Rheol.* 37 (1993) 1057.
- [31] H.M. Laun, H. Münstedt, Elongational behaviour of a low density polyethylene melt. I. Strain rate and stress dependence of viscosity and recoverable strain in the steady state. Comparison with shear data. Influence of interfacial tension, *Rheol. Acta* 17 (1978) 415.
- [32] M.H. Wagner, H. Bastian, P. Hachmann, J. Meissner, S. Kurzbeck, F. Langouche, The strain-hardening behaviour of linear and long-chain-branched polyolefin melts in extensional flows, *Rheol. Acta* 39 (2000) 97.
- [33] G.C. Berry, T.G. Fox, The viscosity of polymers and their concentrated solutions, *Adv. Polym. Sci.* 5 (1968) 261.
- [34] K. Kremer, G.S. Grest, Dynamics of entangled linear polymer melts: a molecular dynamics simulation, *J. Chem. Phys.* 92 (1990) 5057 [Erratum: *J. Chem. Phys.* 94 (1991) 4103].